ADVANCED FUNCTIONAL MATERIALS
www.afm-journal.de

In Situ Monitoring the Role of Working Metal Catalyst Nanoparticles for Ultrahigh Purity Single-Walled Carbon Nanotubes

Tian-Chi Chen, Meng-Qiang Zhao, Qiang Zhang, Gui-Li Tian, Jia-Qi Huang, and Fei Wei**

The high-end applications of single-walled carbon nanotubes (SWCNTs) are hindered by the existence of large amount of impurities, especially the graphene layers encapsulating metal nanoparticles (metal@C NPs). The role of working metal catalysts during chemical vapor deposition (CVD) growth and post purifications by oxidation are not yet fully understood. Herein, the in situ monitoring the role of working metal catalyst NPs for ultrahigh purity SWCNTs by CVD growth and CO_2 purifications is carried out in an online thermogravimetric reactor attached with a mass spectrometer. The growth of SWCNTs almost stops after the initial 2 min, then, the mass increase of the samples mainly originates from the metal@C NP formation. Therefore, high-purity SWCNTs (98.5 wt%) with few metal@C NPs can be available by 2 min CVD growth. Furthermore, CO_2 oxidation of the SWCNTs is also investigated in a thermogravimetric reactor. The oxidation of graphene layers surrounding the metal NPs and the SWCNTs occurs during distinct temperature ranges, which is further demonstrated by the significant differences among their oxidation activation energies. Ultrahigh purity of SWNCT with a carbon content of 99.5 wt% can be available by a CO_2-assited purification method. The in situ study of the CVD growth and CO_2 oxidation of SWCNTs provides the real time information on the working catalyst during reaction and the reactivity information of metal@C NPs and SWCNTs under an oxidizing atmosphere. The success for the preparation of high-purity SWCNT lies in the efficient growth of SWCNTs with a low amount of nanocarbon impurities and partial oxidation of metal@C NPs by catalytic CO_2 oxidation with proper operation parameters.

1. Introduction

Single-walled carbon nanotubes (SWCNTs) are considered as one of the most attractive nanomaterials because of their excellent intrinsic properties, such as high specific surface area, low defect density, and tunable electronic characteristics according to their chirality.[1] Achieving large quantities of SWCNTs with high purity is the first-step to realizing large volume applications, such as fillers for nanocomposites, transparent conductive films, and electrode materials for energy storage.[2,3] The synthesis of SWCNTs has been well achieved by a variety of methods.[1,3–5] However, there are always large amount of impurities, such as amorphous carbon, fullerenes, nanocrystal graphite, and graphene layers encapsulating transition metal nanoparticles (metal@C NPs) in the as-prepared SWCNTs.[5] Such contaminants render it very difficult to understand and to monitor the intrinsic properties of SWCNTs.[6,7] For instance, the SWCNTs are considered as promising candidates as the electrode materials for high-performance double-layer supercapacitors due to their high specific surface area and good structural stability.[8] However, the presence of non-carbon impurities (metal@C NPs) plays a significant role in the decay of the stability of the as-fabricated supercapacitors due to the high reactivity of metal nanoparticles (NPs) to the electrolyte when operating at a high voltage to achieve a high energy density. Therefore, efforts have been devoted to the effective purification of SWCNTs.[6,7] Among the different kinds of impurities, the presence of metal@C NPs is a fundamental challenge for the purification of SWCNTs as metal removal tends to be invariably coupled with a high degree of tube destruction. Although the growth of vertically aligned SWCNTs achieves a very high purity of SWCNTs, scale up of the process is complex.[9,10] As a result, the preparation of high-purity SWCNTs with few metallic impurities has always been a hot topic in carbon nanotube (CNT) technology.

In principle, the growth of SWCNTs and metal@C NPs should have different growth rates due to the fact that SWCNTs always grow on small-sized catalyst NPs, whereas the metal@C NPs are always formed on the NPs with larger size which are usually originated from the sintering of smaller ones.[11,12] Therefore, synthetic methods are expected to prepare SWCNTs

T.-C. Chen, M.-Q. Zhao, Prof. Q. Zhang, G.-L. Tian, Dr. J. Q. Huang, Prof. F. Wei
Beijing Key Laboratory of Green Chemical Reaction Engineering and Technology
Department of Chemical Engineering
Tsinghua University
Beijing 100084, China
E-mail: zhang-qiang@mails.tsinghua.edu.cn; wf-dce@tsinghua.edu.cn

DOI: 10.1002/adfm.201300614

© 2013 WILEY-VCH Verlag GmbH & Co. KGaA, Weinheim

with few metal@C NPs by distinguishing their growth regions. To achieve precise control over the as-grown products, great efforts are turning to real-time in situ and/or operando methods to study the detailed information about the growth process of SWCNTs.[13–16] The use of operando techniques provides real-time information on the working catalyst, which is the cutting-edge catalytic characterization that combined spectroscopic/thermogravimetric (TG) and catalytic information on both homogeneous and heterogeneous catalytic systems.[17] In most cases, Raman spectroscopy is adopted to achieve the in situ/operando study of the dynamics of the nucleation, growth and termination of SWCNTs.[16] However, an in situ/operando Raman study is not expected to distinguish the growth of SWCNTs and metal@C NPs due to the difference in the Raman signals introduced by the growth of metal@C NPs with the presence of large amount of SWCNTs is neglectable. Recent advance in the TG analysis allows the operation of the chemical vapor deposition (CVD) synthesis in a TG reactor. The combination of TG and mass spectroscopy (MS) probe the catalytic information of hydrocarbon conversion as well as the real-time weight of the catalysts, which offer both the TG and catalytic information on heterogeneous catalytic CNT growth systems. Considering the growth of metal@C NPs should give rise to a significant mass increase, real-time in situ/operando TG investigation can be expected to distinguish the growth of SWCNTs and metal@C NPs, and act as a promising effective synthetic method for high-purity SWCNTs.

On the other hand, effective post-purification methods to remove the metal@C NPs without significant destruction on the SWCNTs are also required. Up to now, a variety of strategies have been explored for the purification of SWCNTs, including oxidative methods, chemical functionalization protocols, filtration and chromatography techniques, and microwave heating methods.[6,7,18] Among these, oxidative methods—including liquid phase oxidation treatment, such as acid treatment (HNO_3, $KMnO_4/H_2SO_4$, HCl, etc.) and/or refluxing in water or H_2O_2, as well as gaseous phase oxidation (using O_2, H_2, or air) are mostly used for the large scale purification of SWCNTs.[7] However, such oxidative methods often introduce oxygenated functional groups and serious destruction on the SWCNTs, leading to a low yield of the as-purified SWCNTs. The key issue for the removal of metal@C NPs is to selectively break the graphene layers encapsulated on the metal NPs without destructing the SWCNTs. Recently, it has been reported that the induction of weak oxidant, such as H_2O and CO_2, during the growth of SWCNTs can significantly improve the activity and lifetime of the catalyst.[9,19] The mechanism is supposed to lie in the selective etching of the carbon layers surrounding the catalyst NPs which result in the deactivation of the catalysts. Therefore, the CO_2 oxidation method shows the ability to selectively break the graphene layers on the metal NPs, and act as a promising effective post-purification method for high-purity SWCNTs.

Herein, an in situ TG reactor was employed to probe the growth and CO_2 oxidation of SWCNTs. We demonstrate that controlling the growth of SWCNTs within a very short growth duration can achieve the selective growth of SWCNTs without the formation of large amount of metal@C NPs. In addition, CO_2 oxidation at a proper temperature determined by the in situ TG study was also demonstrated to be effective for the selective oxidation of the graphene layers on metal NPs without significantly damaging the SWCNTs.

2. Results and Discussion

FeMgAl layered double hydroxides (LDHs) were chosen as the catalysts due to their excellent performance for the growth of SWCNTs.[20] The in situ TG study of the growth process for SWCNTs from FeMgAl LDH flakes with a growth duration of 10 min is presented as **Figure 1**a. The growth rate of SWCNTs is determined as the mass increase rate in the TG system. Compared with other routes for in situ growth (such as environmental transmission electron microscopy,[21–23] environmental scanning electron microscopy,[24] X-ray photoelectron spectroscopy,[22,25], optical Imaging,[26] Raman spectra,[13–16] X-ray diffraction,[23] and X-ray reflectivity),[23] the mass increase in TG reactor is very easily detected. There is no press gap between the real CVD reactor and TG analysis for the reason that the reactant feeding gas can be directly introduced without disturbing the monitoring system in the TG reactor. As shown in Figure 1a, the growth of SWCNTs undergoes a very rapid reaction at the beginning. The growth rate of SWCNTs increases rapidly and achieves the largest value of 0.009 $g_{SWCNT}\ g_{cat}^{-1}\ s^{-1}$ at around 27 s. Then, the growth of SWCNTs becomes slower and is almost terminated at around 2 min, probably indicating a very short life-time of the FeMgAl LDH catalysts for SWCNT growth. The mass of the samples still increases gradually during the following 8 min. A total mass increase of 0.45 g is observed during the initial 2 min, but only 0.024 g can be observed for the continued reaction.

To further investigate this phenomenon, samples with a growth duration of 2 and 10 min were collected and characterized. No significant difference in the morphology of the two samples can be observed under SEM characterization (Figure 1b). As shown in Figure 1c, there are large amount of SWCNTs and Fe NPs on the as-calcined FeMgAl layered double oxide (LDO) flakes after a 2-min reaction at 900 °C. No obvious graphene layers can be observed on these Fe NPs as well as on the LDO flakes. This is different from the situation that when a higher growth temperature of 950 °C was adopted, where both graphene layers and SWCNTs can be catalytically deposited on the LDO flakes.[27] However, when the growth duration was extended to 10 min, the formation of large amount of graphene layers encapsulating on the Fe NPs (Fe@C NPs) was observed (Figure 1d). Therefore, we deduce that the mass increase during the initial 2 min was mainly account for by SWCNT deposition, which was almost terminated after the 2-min reaction with an average growth rate of 0.003 $g_{SWCNT}\ g_{cat}^{-1}\ s^{-1}$. The following 8-min reaction corresponded to the further deposition of graphene layers on the Fe NPs to form Fe@C NPs. The graphene layers encapsulated in the Fe NPs acted as blocks between the acid molecules and Fe NPs, preventing them from being removed during the acid treatment. This is supposed to be the main reason for the high Fe content in the SWCNT samples after simple purification. Due to the fact that the CH_4 is a thermally stable carbon source at high temperature, the pyrolysis of amorphous carbon deposited on the raw products is very limited.

© 2013 WILEY-VCH Verlag GmbH & Co. KGaA, Weinheim

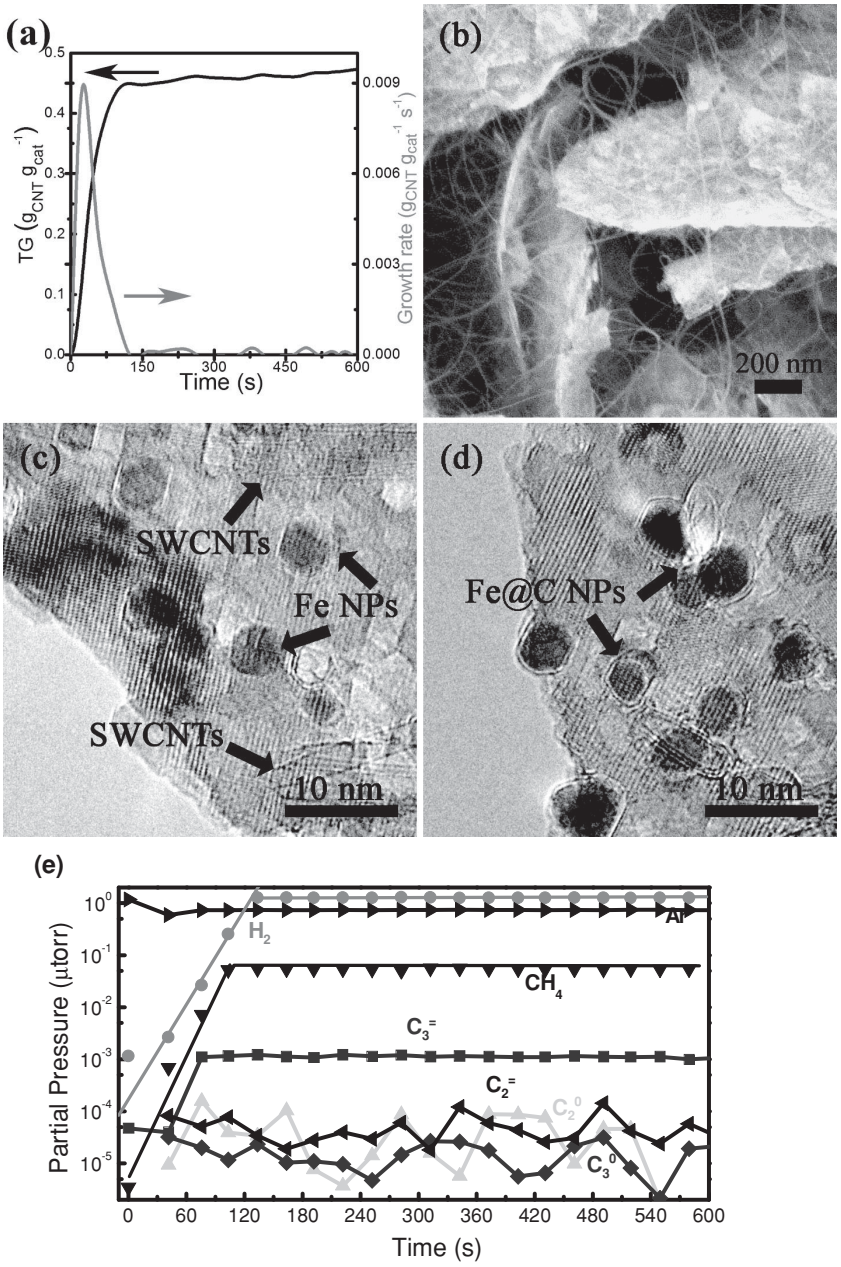

Figure 1. a) TG and DTG curves showing the growth process of SWCNTs from FeMgAl LDH catalysts; b) SEM image showing the morphology of the as-grown SWCNTs on the catalysts; c) TEM image of the Fe NPs after a 2-min growth without the encapsulation of graphene layers; d) TEM image of the obvious Fe@C NPs after a 10-min growth; e) The MS spectrum of the gaseous reactants and products in the TG reactor.

With respect to the above discussion, it was expected that proper reduction on the reaction time for the growth of SWCNTs can effectively reduce the amount of Fe@C NPs, leading to the improved purity of the as-purified SWCNTs after acid treatment without significant reduction in yield. Here, large-scale production of SWCNTs was carried out in a fluidized bed reactor with different reaction durations of 2, 10, and 30 min. The yields of the as-grown SWCNTs were all in a range of 0.43–0.46 g_{SWCNT} g_{cat}^{-1} without significant differences. The as-obtained products were pre-purified by a combined acid and alkali treatments to remove the LDO flakes in the products. TEM images of the corresponding samples after purification, which were denoted as SWCNT-2, SWCNT-10, and SWCNT-30 according to their growth duration, respectively, are shown in **Figure 2**. Compared with SWCNT-2, an increase of the amount of Fe NPs can be observed for SWCNT-10 (Figure 2a,b). When further extending the growth duration to 30 min (SWCNT-30), both the size of the residue Fe NPs and the thickness of the graphene layers encapsulated on them increased significantly (Figure 2c). TGA results shown in Figure 2d reveal that the carbon content of these three samples was 98.5, 92.7, and 90.4%, respectively, indicating a significant increase in purity of the as-purified SWCNTs with decreasing growth duration (Figure 2d). This is in good agreement with the expectation based on the in situ study of the SWCNT growth in TG analyzer mentioned above. Furthermore, it should be noted that the thermal stability of SWCNT-10 greatly decreased in comparison to SWCNT-2. This can be attributed to the presence of a large amount of Fe NPs, which act as a catalyst for the oxidation of nanocarbon. However, the thermal stability of SWCNT-30 exhibited an increase even though they contain slightly more Fe NPs in comparison to SWCNT-2. This can be attributed to the fact that the increasing thickness of the graphene layers encapsulating on the Fe NPs renders them more thermally stable.

Mass spectrometry was used to monitor the real-time gaseous reactant and product concentrations during CNT growth. The initial starting point was set as the introduction of CH_4 to the reduced LDO catalysts. The data were corrected with respect to the background and residual time. A high conversion of CH_4 can be detected at the beginning, however, the concentration increased rapidly during the first 120 s, and then remained constant, which is consistent with the trend of mass increase recorded gravimetrically. Meanwhile, the conversion of CH_4 rapidly decreased. The hydrogen showed a similar trend, indicating the consumption of hydrogen during first stage growth of the SWCNTs. The hydrogen participated in the rapid reduction of the metal NP catalyst. As the hydrogen consumption stopped on the LDH derived catalysts after ≈120 s, the rapid formation of SWCNTs simultaneously ceased. These trends are consistent with the above mentioned two-step growth of SWCNTs and Fe@C NPs. Meanwhile, the ethane, ethylene, propane, as well as propylene could all be detected. The thermal conversion of CH_4 into other hydrocarbons—which is

© 2013 WILEY-VCH Verlag GmbH & Co. KGaA, Weinheim

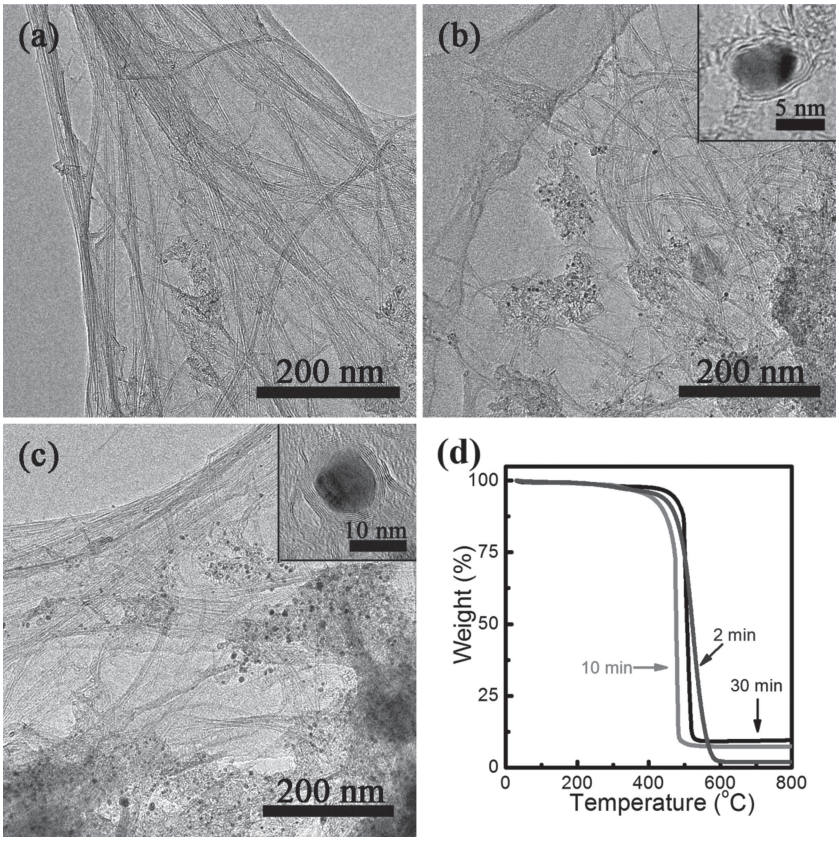

Figure 2. a) TEM image of the SWCNTs after purification for the 3-min growth; b) TEM image of the SWCNTs after purification for the b) 10-min and c) 30-min growth; Inserted images show the morphology of the corresponding Fe@C NPs; d) TGA curves of these three SWCNT samples under O_2 atmosphere.

thermodynamically derived from C-H bonding activation and hydrocarbon transformation and can be detected by ethylene production and pyrolytic carbon formation[28]—was also probed by mass spectrometer during the SWCNT formation at high temperature. The formation mechanism is assumed to be:

$$2CH_4 \longleftrightarrow C_2H_6 + H_2 \quad (1)$$

$$C_2H_6 \longleftrightarrow C_2H_4 + H_2 \quad (2)$$

$$C_2H_4 + CH_4 \longleftrightarrow C_3H_8 \quad (3)$$

$$C_3H_8 \longleftrightarrow C_3H_6 + H_2 \quad (4)$$

The concentration of ethane, ethylene, as well as propane are mostly very low, while the propylene concentration is high and exhibits a similar trend to that of methane. The addition of ethylene into methane enhanced the SWCNT formation, and C_2 is believed to be the most reactive carbon source for CNT formation. The armchair and near-armchair SWCNT systems are reported as the most favorable when the growth mechanism is dominated by reactions such as C_2 addition to the cap rim atoms.[29] Therefore, the ethylene is an intermediate during the SWCNT and other nanocarbon formation, while the propylene presented in relatively high magnification. However, the concentration of propylene is two magnitudes lower than that of methane. During the first stage of rapid SWCNT formation, most of carbon sources converted into SWCNTs. However, with the deactivation of Fe NPs, the conversion of methane, as well as the by-products of propylene is kept at a high concentration during the Fe@C NP formation at the second stage.

The fluidized bed reactor is considered to be the most efficient and effective reactor for SWCNT production.[5] However, it should be mentioned that for the industrial production of SWCNTs, especially for that using routine fluidized bed reactors, it is hard to control the reaction time within 2 min. As a result, the formation of large amount of Fe@C NPs is inevitable. Consequently, effective methods that can remove such Fe@C NPs are required. In principle, the thermal stability of the graphene layers in Fe@C NPs is supposed to be lower than SWCNTs due to the fact that they have better contact with the Fe NPs, which can act as a catalyst for the oxidation of carbon. To fully investigate such differences, the oxidation of SWCNT-30 was studied in situ using a TG analyzer under CO_2 atmosphere with a heating rate of 20 °C min^{-1}. It was observed that the oxidation of SWCNT-30 occurs in three stages, and the corresponding residues are characterized by TEM and Raman spectroscopy (**Figure 3**). As shown in Figure 3a, a weight loss of 8.3% of the sample is observed during Stage I between 747–846 °C. Compared with the initial morphology of the samples (Figure 3b), no significant difference can be found except for the absence of the graphene layers encapsulated on the Fe NPs (Figure 3c). This indicates that Stage I mainly corresponds to the selective oxidation of the graphene layers in Fe@C NPs for SWCNT-30. In this case, CO_2 reacted with solid carbon through reproportionation and generated CO:[30]

$$C + CO_2 \longleftrightarrow CO + C(O) \quad (5)$$

A surface oxygen complex (C(O)) was initially formed and subsequently became stable under the reaction conditions, acting as a retardant by blocking the reaction sites:

$$C(O) \longleftrightarrow C - O \quad (6)$$

It may also decompose and leave the surface as CO

$$C(O) \longleftrightarrow CO \quad (7)$$

Reactions (5–7) depend on the structure of nanocarbon as well as the attached catalyst. Such reaction can be catalytically enhanced by transition metal NPs because CO_2 more readily attacks the carbon/catalyst interface, and the Fe NPs can serve as catalysts for Reaction (5). Fe NPs are thought to modify the electron density and bring reactivity toward oxygen reduction[31] and carbon oxidation under harsh condition. Therefore, the encapsulating graphene can be selectively etched. During Stage II between 846–1070 °C, a significant weight loss of 81.4% for the sample can be observed. TEM image of the sample after

© 2013 WILEY-VCH Verlag GmbH & Co. KGaA, Weinheim

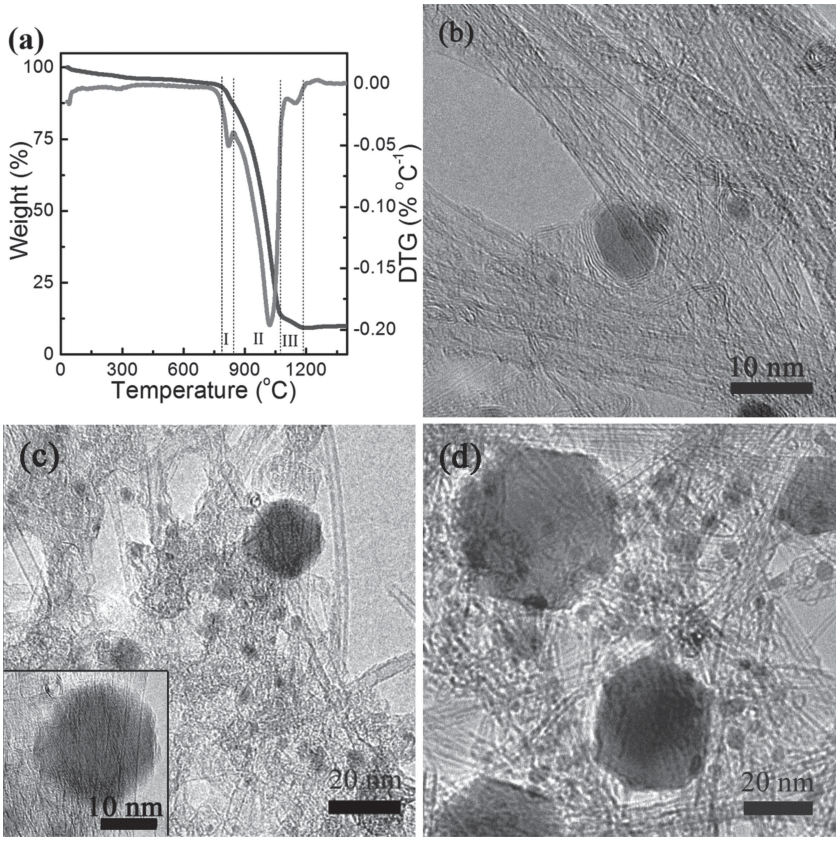

Figure 3. a) TGA curve of the SWCNT-30 after pre-purification under CO_2 atmosphere with a heating rate of 20 °C min^{-1}; b) TEM image of the SWCNT-30 sample; TEM images of the calcined SWCNT-30 under CO_2 atmosphere to c) 907 and d) 1072 °C, the inserted image in (c) shows the high resolution image of the Fe NPs after Stage II.

Stage II shows that the residues are mainly composed of large-size Fe NPs and a small amount of SWCNTs (Figure 3d). This reveals that most of the SWCNTs are oxidized in Stage II, during which sintering of Fe NPs into large particles occurs. No SWCNTs can be found in the samples after Stage III (1070–1090 °C), leaving only iron oxides as the residues. Such different weight loss stages were not observed during TG analysis under an O_2 atmosphere because the oxidation effect of O_2 is too strong to distinguish the different thermal stabilities.

Raman spectra of SWCNT-30 and the residues after Stage I and II are shown in **Figure 4**. The strong radial breath mode (RBM) peaks for all the three samples can be detected, indicating the presence of large quantity of SWCNTs. It was noticed that the value of I_G/I_D increased from an initial value of 3.6 to 8.0 after Stage I, which was further significantly increased to 26.3 after Stage II. The significant increase of the I_G/I_D ratio indicates that the quality of SWCNTs was improved by CO_2 oxidation treatment. The SWCNTs after Stage II are free of attached sp^3 hybridized carbon atoms, leading to strong Stokes scattering, although the amount of SWCNTs is not as high as the raw products. Furthermore, the differed thermal stability for the SWCNTs during Stage II and Stage III may account for their distinguished graphitization. No Raman signals for carbon can be detected for the residues after Stage III.

To investigate the CO_2 oxidation behavior, TG analysis of SWCNTs under CO_2 atmosphere with different heating rates was carried out to obtain the activation energy for graphene layers in Fe@C NPs and SWCNTs. Considering the fact that the migration of Fe NPs during the CO_2 oxidation can induce the oxidation of a large amount of SWCNTs during Stage I with a low heating rate, SWCNT-30 before purification was used because the presence of the LDO flakes can effectively prevent the migration of Fe NPs.[32] Therefore, much more intrinsic values are attained. Three weight loss stages similar with those shown in **Figure 5**a can be observed for TG profiles obtained at different heating rates. As shown in **Table 1**, the position of the three weight loss peaks all moved to higher temperature with the increasing heating rate. This can be attributed to the fact that a faster heating rate makes the oxidation of certain carbon materials complete at a higher temperature. The deformed Arrhenius formula:

$$Ln\frac{\beta}{T_{max}^2} = Ln\frac{AR}{Ea} - \frac{Ea}{RT_{max}} \quad (8)$$

was employed to calculate the activation energies for the different materials based on the position of these three weight loss peaks, in which β is the heating rate, A is the pre-exponential factor, E_a is the activation energy, and T_{max} is the position of the weight loss peak. As shown in Figure 5b, the values of $Ln(\beta T_{max}^{-2})$ exhibited good linear relationship to that of $(-RT_{max})^{-1}$ for all the weight loss peaks. The slopes of the

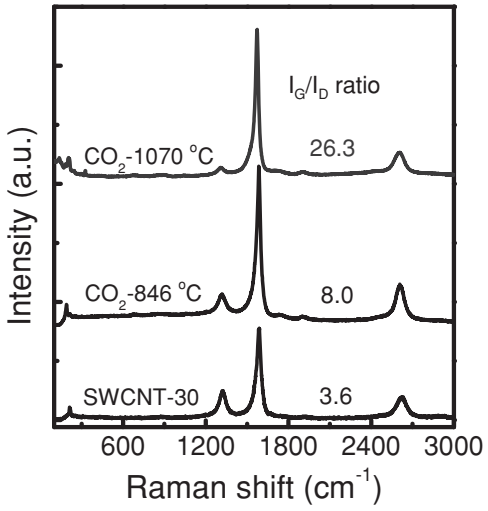

Figure 4. Raman spectra of SWCNT-30, and the products after CO_2 oxidation at different temperatures.

© 2013 WILEY-VCH Verlag GmbH & Co. KGaA, Weinheim

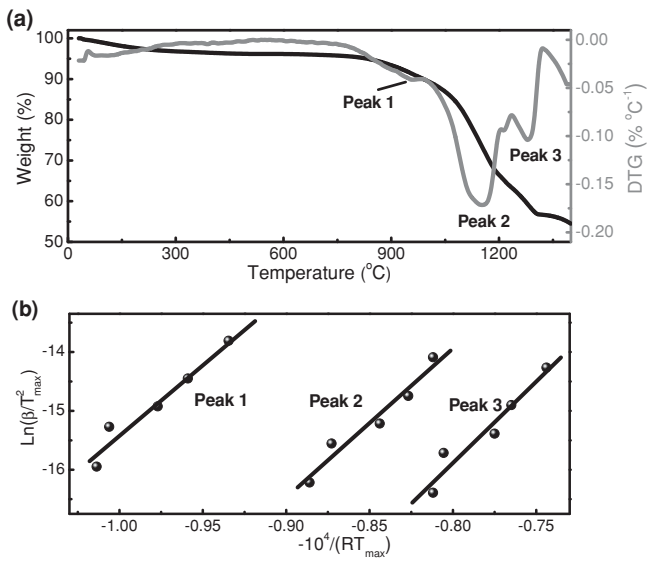

Figure 5. a) TG profiles of CO_2 oxidation of SWCNTs before purification with a heating rate at 30 °C min^{-1}; b) linear fitting charts of the weight loss peaks.

linear fitting curve correspond to the activation energies (E_a). As a result, the calculated E_a of the graphene layers in Fe@C NPs, and SWCNTs in Stage II and III were 240.5, 254.0 and 273.7 kJ mol^{-1}, respectively (Table 1). This further demonstrates that the difference in the thermal stability between Fe@C NPs and SWCNTs can be distinguished by the CO_2 oxidation method. The Fe NPs catalyst was employed as the catalyst for CO_2 gasification during Stage I, therefore, the E_a was the lowest value due to the catalytic gasification by FeNPs. Stage II and III correspond to the oxidation of SWCNTs attached with sp^3 hybridized carbon and perfect sp^2 hybridized SWCNTs, respectively. The highest activation energy corresponded to Stage III which was free of catalytically gasification; consequently, the carbon oxidation rate increased rapidly with the rise of reaction temperature.

Therefore, CO_2 oxidation at a proper temperature is effective for the selective removal of the graphene layers in Fe@C NPs, which can facilitate the improvement of the purity of SWCNTs by subsequent acid treatment. Here, the large-scale produced SWCNTs with a growth duration of 30 min after the pre-purification process (SWCNT-30) were further treated by CO_2 at a temperature of 850 °C for 1 h. The reason we selected the oxidation at 850 °C is because Fe@C NPs can be oxidized at a rapid rate, while the SWCNTs are well preserved (Figure 5a). Consequently, a small weight loss of ca. 10% for the samples was noticed even after such a long period, indicating that the SWCNTs were probably thermally stable during the CO_2 treatment. The morphology of the as-obtained products after subsequent acid washing is shown in **Figure 6**a,b. The products are of high purity of SWCNTs and very few Fe@C NPs can be observed. The TGA curve shown in Figure 6c reveals that a purity of 99.5% can be achieved after the CO_2-assisted purification method, which means that ca. 95% of the Fe NPs in SWCNT-30 has been successfully removed. The Raman spectrum of the products exhibits obvious RBM peaks and a high I_G/I_D value of 18.7, indicating the as-purified SWCNTs have good graphitization. Furthermore, BET analysis reveals that the as-purified SWCNTs have a high specific surface area of 784.6 m^2 g^{-1} and a high total pore volume of 2.3 mL g^{-1}. The success for the preparation of high-purity SWCNTs is attributed to the partial oxidation of Fe@C by catalytic CO_2 oxidation under appropriate operating conditions.

Table 1. Summary of the locations of weight loss peaks in the TG profiles under CO_2 atmosphere at different heating rates.

Heating rate [°C min^{-1}]	10	20	30	50	100	Activation energy [kJ mol^{-1}]
Peak 1	913.5 °C	922.4 °C	958.0 °C	981.2 °C	1014.0 °C	240.5
Peak 2	1084.6 °C	1105.1 °C	1152.3 °C	1181.7 °C	1208.4 °C	254.0
Peak 3	1208.4 °C	1220.0 °C	1278.9 °C	1299.4 °C	1343.9 °C	273.7

3. Conclusions

In situ study of the growth of SWCNTs from FeMgAl LDH catalysts was carried out in a TG reactor. The role of the working LDH catalysts and nanocarbon products can be quantitatively investigated. It was demonstrated that the growth of SWCNTs and Fe@C NPs can be distinguished by controlling the growth duration. By reducing the growth duration from 30 to 2 min, the purity of the as-purified large-scale produced SWCNTs can be improved from 90.4 to 98.5%. Furthermore, results of the in situ TG study of the CO_2 oxidation of SWCNTs revealed that the selective oxidation of the graphene layers surrounding the Fe NPs without obvious destructing the SWCNTs can be achieved, leading to the effective removal of the Fe NPs through the following acid treatment. Consequently, a CO_2-assistant purification process on the as-purified SWCNT-30 was carried out to improve their purity from 90.4 to 99.5%. In contrast to commonly reported CVD growth and purification, high selective growth and efficient purification of SWCNTs with few metal@C NPs were achieved under the guidance of the in situ characterization. The current synthetic method together with CO_2-assiatant post-purification process were both effective for the preparation of large scale high-purity SWCNTs, which is of paramount importance for their practical applications. In addition, such a CVD TG reactor offers opportunities for characterizing the dynamic of CNT formation with high-precision time-resolved mass, which is crucial for probing dynamic changes on catalytically active species and understanding reaction pathways. This approach may also be applicable to systems using other catalytic reaction with product deposition on the working catalyst. Future work will focus on modifying the TG reactor with other characterization ways (e.g. Raman spectrometry or X-ray diffraction) to study the dynamics of SWCNT formation and evolution on the working metal catalyst nanoparticles.

© 2013 WILEY-VCH Verlag GmbH & Co. KGaA, Weinheim

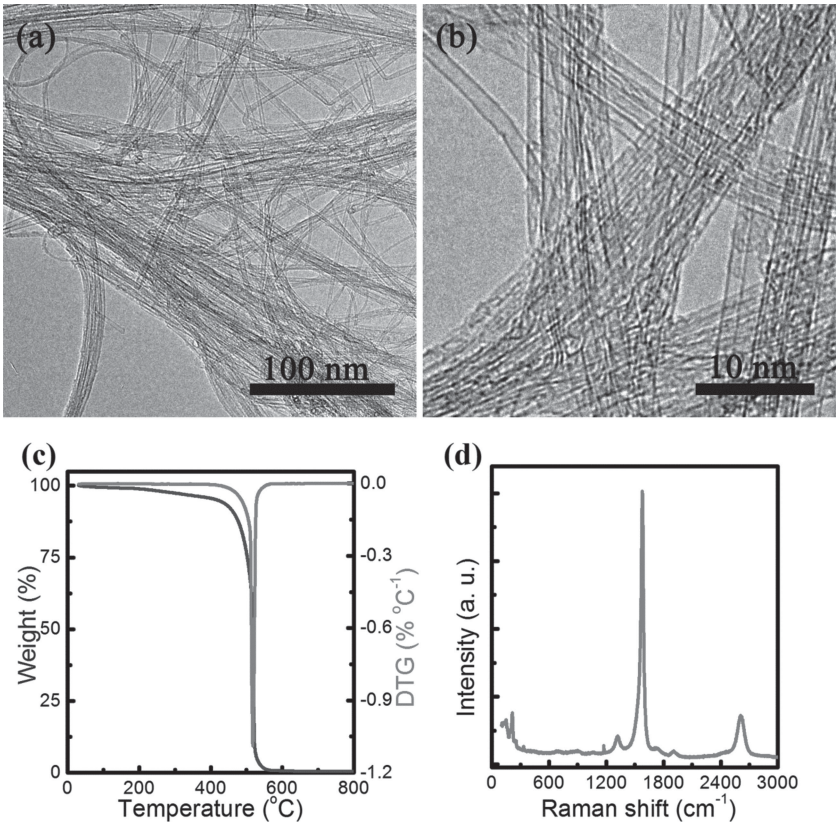

Figure 6. a) SEM image and b) TEM image of the SWCNT-30 after the CO_2 treatment; c) TGA curve under O_2 atmosphere and d) Raman spectra of the SWCNT-30 after the CO_2 treatment.

4. Experimental Section

In Situ Growth of SWCNTs in the TG Reactor: The FeMgAl LDH catalysts were prepared using a urea-assisted co-precipitation reaction which we have previously reported with n(Mg): n(Al): n(Fe) = 3: 1: 0.2.[11] In situ TG study of the SWCNT growth was operated in a TGA/DSC1 STAR^e system. Typically, 2.0 mg FeMgAl LDH flakes were put into a 70 µL Al_2O_3 crucible, which were put into the furnace of the TGA/DSC1 STAR^e system. Then, the furnace was heated to 900 °C with a heating rate of 20 °C min^{-1} under Ar (100 mL min^{-1}) atmosphere. On reaching the reaction temperature, a mixture of H_2/CH_4 with a flow rate of 30/20 mL min^{-1} was introduced into the furnace to start the growth of SWCNTs. The variation of the sample mass was recorded by a record software attached with the TG analyzer and analyzed. A mass spectrometer was combined with the TG reactor to probe the real time gaseous reactants and products during CVD growth of CNTs. A similar process was carried out with the absence of the LDH catalysts to record the mass increase attributed by the formation of amorphous carbon, which served as the baseline for the in situ TG investigation of the SWCNT growth.

Large-Scale Synthesis of SWCNTs: The large scale synthesis of SWCNTs was carried out in a fluidized bed reactor described in our previous report using the FeMgAl LDH catalysts.[11,20] Typically, 2.0 g Fe/Mg/Al LDH catalyst was uniformly fed into the reactor, which was then mounted in an electrical tube furnace and heated to 900 °C under Ar atmosphere with a flow rate of 400 mL min^{-1}. Upon reaching the reaction temperature, H_2 with a flow rate of 100 mL min^{-1} was introduced into the fluidized bed reactor. After 5 min, the flow rate of Ar was turned down to 100 mL min^{-1} and at the same time CH_4 was introduced into the reactor with a flow rate of 400 mL min^{-1} to start the reaction. The reaction duration was controlled as 2, 10, and 30 min, and the corresponding pre-purified products were denoted as SWCNT-2, SWCNT-10, and SWCNT-30, respectively. After the reaction, the fluidized bed reactor was cooled down to room temperature under Ar atmosphere. The as-obtained products were then collected for further purification and characterization.

Purification of the SWCNTs: The large-scale produced SWCNTs were pre-purified with a combined alkali and acid treatments to remove the metal oxides originated from the calcination of the LDH flakes. Typically, the samples were first treated hydrothermally by NaOH solution (15 mol L^{-1}) at a temperature of 150 °C for 8 h. After that, the as-obtained products were then immersed into HCl solution (3 mol L^{-1}) at a temperature of 80 °C for 3 h. The as-obtained products were then filtered, washed by deionized water, and dried in oven at 100 °C for 12 h, leaving the pre-purified SWCNTs.

The pre-purified SWCNT-30 were further purified by a CO_2-assistant purification method to remove the residue Fe@C NPs. Typically, the pre-purified SWCNT-30 were treated by CO_2 (50%) and Ar (50%) at 850 °C for 1 h. Then, the as-obtained products were treated by HCl solution (3 mol L^{-1}) at 80 °C for 3 h to further remove the Fe NPs in the samples. The as-obtained products were filtered, washed, and dried for further characterization.

In Situ TG Investigation of the Oxidation of SWCNTs: The oxidation study of the samples was studied in the TGA/DSC1 STAR^e system under O_2 or CO_2 atmosphere. Typically, about 5 mg samples were put into a 70 µL Al_2O_3 crucible, which were put into the furnace of the TGA/DSC1 STAR^e system. For the O_2 oxidation treatment, the furnace was heated from 30 to 900 °C with a heating rate of 20 °C min^{-1} under a mixture of N_2/O_2 (50/50 mL min^{-1}) atmosphere. For the CO_2 oxidation study, the furnace was heated from 30 to 1400 °C with different heating rates of 10, 20, 30, 50, 100 °C min^{-1}.

Characterization: The morphology of the samples were characterized by a JSM 7401F (JEOL Ltd., Tokyo, Japan) SEM operated at 3.0 kV and a JEM 2010 (JEOL Ltd, Tokyo, Japan) TEM operated at 120.0 kV. The BET specific surface area of the samples were measured by N_2 adsorption/desorption using Autosorb-IQ2-MP-C system. Raman spectra were recorded with He-Ne laser excitation at 633 nm using Horiba Jobin Yvon LabRAM HR800 Raman Spectrometer.

Acknowledgements

The work was supported by the Foundation for the China National Program (No. 2011CB932602) and Beijing City Innovative Scientific Program (20121097711).

Received: February 17, 2013
Published online: May 22, 2013

[1] a) W. Y. Zhou, X. D. Bai, E. G. Wang, S. S. Xie, *Adv. Mater.* **2009**, *21*, 4565; b) E. Joselevich, H. Dai, J. Liu, K. Hata, A. H. Windle, *Top. Appl. Phys.* **2008**, *111*, 101.
[2] a) M. F. L. De Volder, S. H. Tawfick, R. H. Baughman, A. J. Hart, *Science* **2013**, *339*, 535; b) Q. Zhang, J. Q. Huang, W. Z. Qian, Y. Y. Zhang, F. Wei, *Small* **2013**, *9*, 1237.

© 2013 WILEY-VCH Verlag GmbH & Co. KGaA, Weinheim

[3] a) Z. Liu, L. Jiao, Y. Yao, X. Xian, J. Zhang, *Adv. Mater.* **2010**, *22*, 2285; b) Y. Ma, B. Wang, Y. Wu, Y. Huang, Y. Chen, *Carbon* **2011**, *49*, 4098.
[4] a) J. P. Tessonnier, D. S. Su, *ChemSusChem* **2011**, *4*, 824; b) H. W. Zhu, C. L. Xu, D. H. Wu, B. Q. Wei, R. Vajtai, P. M. Ajayan, *Science* **2002**, *296*, 884.
[5] Q. Zhang, J.-Q. Huang, M.-Q. Zhao, W.-Z. Qian, F. Wei, *ChemSusChem* **2011**, *4*, 864.
[6] P. X. Hou, C. Liu, H. M. Cheng, *Carbon* **2008**, *46*, 2003.
[7] T. J. Park, S. Banerjee, T. Hemraj-Benny, S. S. Wong, *J. Mater. Chem.* **2006**, *16*, 141.
[8] a) A. Izadi-Najafabadi, S. Yasuda, K. Kobashi, T. Yamada, D. N. Futaba, H. Hatori, M. Yumura, S. Iijima, K. Hata, *Adv. Mater.* **2010**, *22*, E235; b) X. Li, J. P. Rong, B. Q. Wei, *ACS Nano* **2010**, *4*, 6039.
[9] K. Hata, D. N. Futaba, K. Mizuno, T. Namai, M. Yumura, S. Iijima, *Science* **2004**, *306*, 1362.
[10] Y. Murakami, S. Chiashi, Y. Miyauchi, M. H. Hu, M. Ogura, T. Okubo, S. Maruyama, *Chem. Phys. Lett.* **2004**, *385*, 298.
[11] M.-Q. Zhao, Q. Zhang, X.-L. Jia, J.-Q. Huang, Y.-H. Zhang, F. Wei, *Adv. Funct. Mater.* **2010**, *20*, 677.
[12] M.-Q. Zhao, Q. Zhang, J.-Q. Huang, F. Wei, *Adv. Funct. Mater.* **2012**, *22*, 675.
[13] R. Rao, N. Pierce, D. Liptak, D. Hooper, G. Sargent, S. L. Semiatin, S. Curtarolo, A. R. Harutyunyan, B. Maruyama, *ACS Nano* **2013**, *7*, 1110.
[14] M. Picher, E. Anglaret, R. Arenal, V. Jourdain, *Nano Lett.* **2009**, *9*, 542.
[15] R. Rao, D. Liptak, T. Cherukuri, B. I. Yakobson, B. Maruyama, *Nat. Mater.* **2012**, *11*, 213.
[16] P. Finnie, A. Li-Pook-Than, J. Lefebvre, *Nano Res.* **2009**, *2*, 783.
[17] a) O. Diebolt, P. van Leeuwen, P. C. J. Kamer, *ACS Catal.* **2012**, *2*, 2357; b) F. Tao, *ChemCatChem* **2012**, *4*, 583; c) S. J. Tinnemans, J. G. Mesu, K. Kervinen, T. Visser, T. A. Nijhuis, A. M. Beale, D. E. Keller, A. M. J. van der Eerden, B. M. Weckhuysen, *Catal. Today* **2006**, *113*, 3.
[18] a) A. R. Harutyunyan, B. K. Pradhan, J. P. Chang, G. G. Chen, P. C. Eklund, *J. Phys. Chem. B* **2002**, *106*, 8671; b) L. M. Sheng, L. Shi, K. An, L. M. Yu, Y. Ando, X. L. Zhao, *Chem. Phys. Lett.* **2011**, *502*, 101.
[19] J. Q. Huang, Q. Zhang, M. Q. Zhao, F. Wei, *Nano Res.* **2009**, *2*, 872.
[20] a) M.-Q. Zhao, G.-L. Tian, Q. Zhang, J.-Q. Huang, J.-Q. Nie, F. Wei, *Nanoscale* **2012**, *4*, 2470; b) M.-Q. Zhao, Q. Zhang, J.-Q. Huang, J.-Q. Nie, F. Wei, *Carbon* **2010**, *48*, 3260.
[21] a) S. Helveg, C. Lopez-Cartes, J. Sehested, P. L. Hansen, B. S. Clausen, J. R. Rostrup-Nielsen, F. Abild-Pedersen, J. K. Norskov, *Nature* **2004**, *427*, 426; b) S. Hofmann, R. Blume, C. T. Wirth, M. Cantoro, R. Sharma, C. Ducati, M. Havecker, S. Zafeiratos, P. Schnoerch, A. Oestereich, D. Teschner, M. Albrecht, A. Knop-Gericke, R. Schlogl, J. Robertson, *J. Phys. Chem. C* **2009**, *113*, 1648.
[22] a) S. Hofmann, R. Sharma, C. Ducati, G. Du, C. Mattevi, C. Cepek, M. Cantoro, S. Pisana, A. Parvez, F. Cervantes-Sodi, A. C. Ferrari, R. Dunin-Borkowski, S. Lizzit, L. Petaccia, A. Goldoni, J. Robertson, *Nano Lett.* **2007**, *7*, 602; b) S. A. Steiner, T. F. Baumann, B. C. Bayer, R. Blume, M. A. Worsley, W. J. MoberlyChan, E. L. Shaw, R. Schlogl, A. J. Hart, S. Hofmann, B. L. Wardle, *J. Am. Chem. Soc.* **2009**, *131*, 12144.
[23] C. T. Wirth, B. C. Bayer, A. D. Gamalski, S. Esconjauregui, R. S. Weatherup, C. Ducati, C. Baehtz, J. Robertson, S. Hofmann, *Chem. Mater.* **2012**, *24*, 4633.
[24] I. Wako, T. Chokan, D. Takagi, S. Chiashi, Y. Homma, *Chem. Phys. Lett.* **2007**, *449*, 309.
[25] a) C. Mattevi, C. T. Wirth, S. Hofmann, R. Blume, M. Cantoro, C. Ducati, C. Cepek, A. Knop-Gericke, S. Milne, C. Castellarin-Cudia, S. Dolafi, A. Goldoni, R. Schloegl, J. Robertson, *J. Phys. Chem. C* **2008**, *112*, 12207; b) A. Rinaldi, J. P. Tessonnier, M. E. Schuster, R. Blume, F. Girgsdies, Q. Zhang, T. Jacob, S. B. A. Hamid, D. S. Su, R. Schlogl, *Angew. Chem. Int. Ed.* **2011**, *50*, 3313.
[26] a) A. J. Hart, L. van Laake, A. H. Slocum, *Small* **2007**, *3*, 772; b) E. Einarsson, Y. Murakami, M. Kadowaki, S. Maruyama, *Carbon* **2008**, *46*, 923; c) K. Hasegawa, S. Noda, *ACS Nano* **2011**, *5*, 975; d) J. Q. Huang, Q. Zhang, M. Q. Zhao, K. Zhou, F. Wei, *Carbon* **2011**, *49*, 1395.
[27] M. Q. Zhao, X. F. Liu, Q. Zhang, G. L. Tian, J. Q. Huang, W. C. Zhu, F. Wei, *ACS Nano* **2012**, *6*, 10759.
[28] a) P. Lucas, A. Marchand, *Carbon* **1990**, *28*, 207; b) Z. J. Hu, K. J. Hüttinger, *Carbon* **2003**, *41*, 1501.
[29] D. A. Gomez-Gualdron, P. B. Balbuena, *J. Phys. Chem. C* **2009**, *113*, 698.
[30] H. Marsh, F. Rodriguez-Reinoso, *Activated Carbon*, Elsevier, Amsterdam **2006**, 243.
[31] a) D. H. Deng, L. Yu, X. Q. Chen, G. X. Wang, L. Jin, X. L. Pan, J. Deng, G. Q. Sun, X. H. Bao, *Angew. Chem. Int. Ed.* **2013**, *52*, 371; b) Y. G. Li, W. Zhou, H. L. Wang, L. M. Xie, Y. Y. Liang, F. Wei, J. C. Idrobo, S. J. Pennycook, H. J. Dai, *Nat. Nanotechnol.* **2012**, *7*, 394.
[32] M.-Q. Zhao, Q. Zhang, W. Zhang, J.-Q. Huang, Y. Zhang, D. S. Su, F. Wei, *J. Am. Chem. Soc.* **2010**, *132*, 14739.

© 2013 WILEY-VCH Verlag GmbH & Co. KGaA, Weinheim